

Full Length Research Paper

Theoretical and conceptual derivation of threshold phenomena and metabolic switching models in a chemostat system

Jacques Thierie

ULB Guest Auditor - (Faculté des Sciences) – Independent Researcher, Rue de Beysehem 248, 1120
Bruxelles – Belgium.

Received 1 August, 2018; Accepted 8 October, 2018

A chemostat cell culture is a polyphasic dispersed system. Three models using net transport and metabolization (T/M) kinetics of hyperbolic form have been described. The first uses only one metabolic pathway and has been studied under various conditions. The second uses two metabolic pathways, with either high or low affinity for the substrate. The third adds excretion of fermentative products to the pathways in model two. Examining the steady states at various dilution rates (D) reveals a critical value (threshold value, D_c), at which the substrate can abruptly invade the cells. If the substrate or its derivatives are active, this abrupt concentration increase may act as a signal at particular growth rates. The second model has been used to study cases where the extracellular compound is a limiting substrate. When part of the substrate was excreted in the form of metabolites, there was a sharp transition between the anabolic and excretion pathways. The excretion pathways are abruptly activated above a critical growth rate. In all cases, the “threshold effects” were related to global and intrinsic characteristics of the culture, represented by the formula $D_c = Y_{X^c,S} V_S^0$. This result may be of practical importance for designing and optimizing biotechnological processes in continuous cultures. The derived model has been effectively used to describe the Crabtree effect in *Saccharomyces cerevisiae*, which likely implies at least two input pathways of the substrate. The weak affinity pathway is responsible for the respiratory-reproductive transition and leads to the excretion of the fermentation products, including ethanol in yeast and lactate for certain cancers.

Key words: Threshold, metabolic switch, Crabtree effect, substrate transport, respiro-fermentative transition.

INTRODUCTION

The interest of modeling in biotechnology is well established and the field of research has been developed considerably in an attempt to meet an unceasingly growing need (sometimes related with Biosystems) (FOCAPD, 2004). The main driving force for model

development is undoubtedly the requirement to provide an adequate representation of the increasingly complex phenomena that are available, for both therapeutic and economic reasons.

Based on the analysis of Bellgardt (1991), the

E-mail: thieriej@gmail.com. Tel: +32(0)2 268 04 68.

Author(s) agree that this article remain permanently open access under the terms of the [Creative Commons Attribution License 4.0 International License](https://creativecommons.org/licenses/by/4.0/)

unstructured models that present a global description of the phenomena at the bioreactor level become limited as soon as additional information about cellular dynamics is required. The structured models, which take into account various details concerning the physiological organization of the cell, provide a local description that allows for the representation of more complex phenomena. These models however, remain imprecise in terms of intracellular dynamics. In the case of compartmented structured models, the complexity of the models increases in a prohibitory way according to the number of compartments, which limits their practical exploitation. Among others, models known as cybernetic or “metabolic regulators” emerged in the 1980s to describe growth phenomena on multiple substrates media. These models are more focused on the local description of intracellular kinetics and were shown to successfully represent several complex phenomena. The main objection concerning the latter two types of modeling relates to the way these models highlight the regulation of metabolism. Indeed, they call upon very general optimization concepts, such as growth rate maximization (Giuseppin and van Riel, 2000), the legitimacy of which is not necessarily recognized (Varma and Palsson, 1993a, 1993b). How the regulation is carried out has not been addressed, and the optimization procedures rely on the fact that biological evolution was supposedly responsible for choosing the optimal process (Bellgardt, 1991). Technically speaking, the consequence of this conceptualization implies that, at any given moment of the system evolution, several options may arise. To meet this situation, the “model-builder” must introduce some conditional tests in his or her algorithm and choose the option that best corresponds to the “pre-established” optimization criterion.

Growth on multiple substrates, also known as diauxie, is one of the main phenomena that led to this kind of modeling (Zhang et al., 2017). The problem that arises is then to represent the “switch” correctly that allows for the consumption of a second, less “favored” substrate after the exhaustion of the first substrate. Models with compartments are able to describe this kind of phenomena because the transitions are sufficiently “smooth”; unstructured, cybernetic and metabolic regulator-based models require a priori-defined conditional tests, discontinuous functions, or optimization criteria.

The model we present here is a new approach to depict the “switch” phenomena occurring between various metabolic pathways and avoids both pre-established discontinuous functions and optimization criteria. It is based on the fact that some realistic kinetics possess the intrinsic property of activating various metabolic pathways in response to constraints imposed by the culture conditions, without any “*ad hoc*” precondition. The possible transitions can be “smooth,” but also extreme and describe threshold phenomena well. The model therefore leads to concepts close to the metabolic flux analysis (MFA) (Schügerl and Bellgardt, 2000), but avoids

deep knowledge of metabolism biochemical reactions. The transport/metabolization rates initially obtained in an implicit form within the polyphasic dispersed systems framework (PDS) (Thierie, 1997) are reported explicitly using this method.

This study has been carried out in cultures at a level that is between the level of the reactor and that of intracellular reactions

Consequently, the explicit form of the transport/metabolization reactions allows us to calculate and represent the specific rates associated with the metabolism of the cellular phase. The results presented here concern systems in a steady state, but the model itself could be applied to transient phenomena, as long as the depicted process takes place on a sufficiently slow time scale to validate the quasi-steady state assumption.

MATERIALS AND METHODS

The biphasic “chemostat”

Only continuous cultures systems, in particular simple chemostat were considered. After several developmental setbacks in the last 70 years, chemostat and its derivative (turbidostat, retentostat, statiostat, etc.) culture systems have progressed considerably. These systems have been used for many applications including low-cost cultures such as yeast (Matteau et al., 2015; Payen and Dunham, 2017), biological evolution analysis (Gresham and Hong, 2015), microbial systems (Ziv et al., 2013), etc. More sophisticated models such as that of Zhang et al. (2017), Rapaport et al. (2018), etc., have also been developed.

However, the scope of this work is to consider a biphasic “chemostat,” made up solely of one cellular phase (of superscript c) and a liquid “phase” (the culture medium), called matrix (of superscript m). The usual working conditions of the chemostat are as follows: (1) the working volume, V_T , is constant; (2) the influent volumetric flow is constant and equal to the effluent flux, $Q^E=Q^S=Q$; (3) the compound concentration in the feed $\tilde{C}_S^{m,E}$ is constant; (4) the cellular phase consists of only one cellular species (pure strain); (5) the cellular viability is close to 100%; (6) there are no cells in the influent.

To these usual conditions, the following were added:

- (1) The average cellular specific mass δ_c is independent of the growth rate;
- (2) The average water content of the cells is constant and independent of the growth rate.

These two factors showed that they could play a role in both physiological kinetics and in mass balances, on which the yield coefficient depends. The discussion of these two conditions is the basis of this study. Hereafter, the term “flux” refers to any quantity represented by mass per volume and by the unit of time, and the “specific rate,” is the flux value divided by the biomass. Therefore, the specific rate is the flux per biomass unit (units: h^{-1} , for example).

Implicit mass balance

Cellular phase

Let us consider a constant volume biphasic “chemostat.” For a

compound S, transported from the dispersing matric phase m towards the micellar (cellular) phase c , the implicit mass balance in the cellular phase is, in term of pseudo-homogeneous concentrations (Thierie, 1997):

$$\frac{d\tilde{C}_S^c}{dt} = -D\tilde{C}_S^c + \Phi_{S,m}^0(c) - q_S^c(\cdot)X^c + \tilde{C}_S^c \frac{d \ln N_T^c}{dt} \quad (1)$$

where $D = Q/V_T$ is the dilution rate; \tilde{C}_S^c is the pseudo-homogeneous compound concentration in the cellular phase; $\Phi_{S,m}^0(c)$ is the total interphasic exchange flux (in the direction $m \rightarrow c$) per volume unit;

$q_S^c(\cdot)$ is the specific transport/metabolization rate of the compound in the cellular phase (the notation (\cdot) points to a complex function, possibly depending on many factors; this bracket has been omitted at several instances); X^c is the biomass; N_T^c is the total cells number.

If necessary, more details on the formalism can be obtained in Thierie (2016). The steady state of Equation 1 is then

$$\Phi_{S,m}^0(c) = q_S^c(\cdot)X^c + D\tilde{C}_S^c \quad (2)$$

which expresses that the interphasic transfer flux per unit of volume is equal to the sum of the net metabolization specific rate of the compound multiplied by the biomass plus the exhaust term of the chemostat. This last term expresses the intracellular compound outlet associated with the hydraulic cells outlet.

The relation (Equation 2) can be put in the form ($q_S^c \equiv q_S^c(\cdot)$)

$$q_S^c = \frac{\Phi_{S,m}^0(c)}{X^c} - \frac{D\tilde{C}_S^c}{X^c} \quad (3)$$

Using the definition of the yield coefficient related to S

$$Y_{X^c,S} = \frac{X^c}{\tilde{C}_S^{m,E} - \tilde{C}_S^m} \quad (4)$$

and the compound mass fraction (intracellular mass of compound per biomass unit)

$$\alpha_S^c = \frac{\tilde{C}_S^c}{X^c} \quad (5)$$

it comes that

$$q_S^c = D \left(\frac{1}{Y_{X^c,S}} - \alpha_S^c \right) \quad (6)$$

This relation is always true for a transport phenomenon followed by consumption. The relations (Equations 3 and 6) express that the effective transport/metabolization rate is the difference between the specific interphasic transport flux and the compound outlet associated with the cells that leave the reactor. The effective transport/metabolization rate is thus not directly observable and can only be calculated if the intracellular concentration is known.

With

$$0 \leq \alpha_S^c < \alpha_{S,\max}^c \quad (7)$$

Theoretically, the maximum value of $\alpha_{S,\max}^c$ is 1. Nevertheless, this implies that the cellular phase is only made of intracellular compounds, which is not the case. Realistic values of $\alpha_{S,\max}^c$; however, are occasionally very high for the compounds that are hard to metabolize or during storage. Unity then constitutes the absolute upper value (theoretical limit).

The extreme values (minimum and maximum) of the metabolization rate are thus determined by upper and lower limits (Equation 7), whereby

$$\min(q_S^c) = D \left(\frac{1}{Y_{X^c,S}} - \alpha_{S,\max}^c \right) \quad (8)$$

and ($\alpha_S^c = 0$; completely metabolized compound)

$$\max(q_S^c) = \frac{D}{Y_{X^c,S}} \quad (9)$$

This last equation is very important when the compound S is the limiting substrate.

Notably, when the intracellular concentration is very low compared to the inverse of the yield coefficient, the relation (Equation 3) indicates that the specific transfer flux is equal to the rate of disappearance of the compound. In this case, relation (Equation 9) shows that this consumption rate versus dilution rate is a straight line going through the origin and with an equal slope to the inverse of the yield coefficient. In experiments, if S is the limiting substrate, it is not always the case and some cultures show a line that does not pass through the origin. This substrate consumption associated with null growth ($D = 0$) is generally interpreted in terms of cellular maintenance energy (Pirt, 1965; Pirt, 1982; Tempest and Neijssel, 1984). In this work, the problematic concept of maintenance will not be introduced. A discussion of this problem within the PDS framework can be found elsewhere (Thierie, 2000; Kempes et al., 2017; Vos et al., 2016).

Matric phase

In the dispersing matric phase, the compound mass balance is

$$\frac{d\tilde{C}_S^m}{dt} = D(\tilde{C}_S^{m,E} - \tilde{C}_S^m) - \Phi_{S,m}^0(c) \quad (10)$$

where $\tilde{C}_S^{m,E}$ and \tilde{C}_S^m are the compound concentrations in the matric phase at the inlet and in the bulk of the reactor, respectively. In the steady state

$$\Phi_{S,m}^0(c) = D(\tilde{C}_S^{m,E} - \tilde{C}_S^m) \quad (11)$$

which expresses that the flux transferred towards the cellular phase is simply the difference between the entering and the outgoing flux in the bioreactor.

RESULTS

The transport of microbial sugars is a complex process often linked to the catabolism of the sugars themselves (Afroz et al., 2014). This observation was integrated as a general entangled mechanism. Thus, a plural mechanism is defined by a single "step," as the following.

Transport/Metabolization kinetics (T/M)

The total net specific rate allowing compound metabolization into the cell is the result of several processes: (a) compound diffusion from the matric phase towards the membrane; (b) compound transport from outside to inside the cell; (c) compound metabolization (complete or not) in the cell.

The rate resulting from these three processes will be referred to as transport/metabolism (T/M). Similar considerations about transport and metabolism synchronism can be found in McCoy et al. (2015).

Substrate diffusion in the external layer of the cell results in the expression of the T/M specific rate in term of local concentration (Coulson and Richardson, 1987), that is, in terms of "reactive concentration" (or R-concentration) (Thierie, 1997; Thierie, 2016). Therefore, the general implicit expression of this specific rate takes the following form:

$$q_S^c = f(C_S^c, \dots) \quad (12)$$

where C_S^c is a R-concentration.

As a net rate, this relation can always be decomposed into a set of terms that take the multiplicity of transport ways and the diversity of the metabolic pathways into account:

$$q_S^c = \sum_i f_i(C_S^c, \dots) \quad (13)$$

An explicit form of Equation 13 can be obtained by using a very general hyperbolic function to represent the specific T/M rate:

$$q_S^c = \sum_{i=1}^n \frac{V_S^0(i) C_S^c}{K_S(i) + C_S^c} \quad (14)$$

where $V_S^0(i)$ is the maximum T/M rate for pathway i and $K_S(i)$ is the "affinity" for the compound corresponding to this pathway (affinity is the inverse of the constant). Weusthuis et al. (1994) already used similar kinetics for the description of transport phenomena making use of multiple carriers. Similar considerations can be found in

Koch (1997), although more sophisticated and more general ones are also described.

To increase the clarity of the argument, we will proceed in order of increasing complexity by examining the systems with: (1) one substrate transport pathway; (2) two substrate transport pathways; (3) two substrate transport pathways supplemented by the excretion of a secondary metabolite.

A two-way transport system with excretion of a single secondary metabolite represents the simplest realistic situation. Notably, more than two transport systems can exist (McCoy et al., 2015; Degnan et al., 2014) and the excretion of several metabolites is common (Green and Mecsas, 2016; Dzialo et al., 2017). Our simplified system, however, captures most of the phenomena we aim to represent.

$n=1$: One-way model

Relation between R- and E-concentrations (Thierie, 1997) is given by:

$$C_S^c = \tilde{C}_S^c \frac{\delta_c}{X^c} \quad (15)$$

where δ_c is the volumetric mass (g/l) of the cellular phase.

Applying this relation to Equation 14 for $n=1$, it is easy to show that

$$q_S^c = \frac{V_S^0 \tilde{C}_S^c}{K_S^* X^c + \tilde{C}_S^c} \quad (16)$$

where $V_S^0 = V_S^0(1)$ and $K_S^* = K_S(1)/\delta_c$ (note that K_S^* has no unit).

The characteristic of Equation 16 is to show that the total affinity $K_S^* X^c$ ceases to be a constant and becomes biomass-dependent. This property was reported by several authors and has been justified within the collisional limit framework (Abbott and Nelsestuen, 1988). This point will be reconsidered in the discussion.

Using Equation 16 in the implicit mass balance (Equation 2), we obtain the steady state

$$\Phi_S^0 = \frac{V_S^0 \tilde{C}_S^c}{K_S^* X^c + \tilde{C}_S^c} X^c + D \tilde{C}_S^c \quad (17)$$

where $\Phi_S^0 \equiv \Phi_{S,m}^0(c)$, Φ_S^0 , X^c and D are easily observable experimental data; \tilde{C}_S^c is the pseudo-homogeneous concentration of the compound S which can be

calculated in the steady state using Equation 17 to satisfy the mass balance. This expression can be put in a polynomial form with variable coefficients:

$$P^2(\tilde{C}_S^c) \equiv a_2(\tilde{C}_S^c)^2 + a_1\tilde{C}_S^c + a_0 = 0 \quad (18)$$

with

$$\begin{aligned} a_0 &= -K_S^* X^c \Phi_S^0 \\ a_1 &= X^c (V_S^0 + DK_S^*) - \Phi_S^0 \\ a_2 &= D \end{aligned} \quad (19)$$

It can be shown that Equation 18 always admits only one real not negative root

$$\tilde{C}_S^c = \frac{-a_1 + \sqrt{a_1^2 - 4a_2a_0}}{2a_2} \quad (20)$$

and a zero solution for the trivial cases $X^c = 0$ and $\Phi_S^0 = 0$.

To investigate the properties of Equation 18, it is necessary either to have experimental data or to use a "data generator model."

This last solution will be applied, using the Monod's model (Doran, 1995), which allows data to be generated in the following way. In the steady state:

$$S = \frac{K_M D}{\mu_{max} - D} \quad (21a)$$

$$X = Y_M (S^0 - S) \quad (21b)$$

These relations are valid, provided that D is lower than the washout dilution rate:

$$D_W = \frac{\mu_{max} S^0}{K_M + S^0} \quad (21c)$$

For $D > D_W$, one assumes that $X = 0$ and $S = S^0$ (S^0 : S : the substrate in the inlet and in the bulk of the reactor; X : biomass; Y_M : yield coefficient; μ_{max} : maximum specific growth rate; K_M : half-saturation constant). With the provision that cellular density is not too high, we can adopt the following approximations: $X^c \approx X$, $\tilde{C}_S^m \approx S$ and $\tilde{C}_S^{m,E} \approx S^0$.

Using relation (Equation 21a,b,c), it is possible to test the properties of Equation 18. It was revealed that two types of qualitatively different situations can arise according to the value of V_S^0 .

Case where $V_S^0 > D_W$ (high specific T/M rate)

Figure 1a shows the compound profile in the cellular phase. The model cannot distinguish if the compound is adsorbed or if it has penetrated the cells.

There is a continuous increase in the compound concentration up to a specific value of D , followed by an abrupt decrease. The K_S^* value controls the order of magnitude of \tilde{C}_S^c over the whole interval of D . The concentration in the cellular phase decreases when affinity increases. When K_S^* tends towards zero, the concentration also tends towards zero.

Figure 1b shows that the net specific rate, q_S^c , tends towards its maximum when affinity tends towards infinite ($K_S^* = 0$). It should be noted that on using Equation 9, the following relation is obtained:

$$\max(q_S^c) = \frac{\Phi_S^0}{X^c} = \frac{D}{Y_{X^c,S}} = \frac{D}{Y_M} \quad (22)$$

In other words, the system maximum rate tends towards one of the generator models. It should, however, be noted that Y_M is no more than an empirical parameter intended to simulate the experimental values. Within the context of the system, it does not have a precise meaning; it is only a special value of $Y_{X^c,S}$, the "true" yield coefficient of the system.

Case where $V_S^0 < D_W$ (weak specific T/M rate)

When the maximum T/M specific rate is smaller than the washout dilution rate, the situation changes completely. Figure 2a shows that variation of the compound concentration increases compared to that in the previous situation (Figure 1a). Moreover, increasing affinity leads to the formation of two distinct regions. At low dilution rates, concentration in the cellular phase tends towards zero; at high dilution rates, it tends towards a positive value, and is not very sensitive to K_S^* .

Figure 2b shows that this effect is due to T/M specific rate saturation at high affinities, which intervenes around a critical value, D_c . For $D < D_c$, the rate quickly reaches a value close to its maximum (Equation 22). Beyond this value, the specific rate "saturates" at V_S^0 , and the compound accumulates in the cellular phase. A highly differentiated concentration in the internal substrate concentration (or its derivatives) as shown in Figure 2b could give rise to flux-sensing phenomena possibly regulating important metabolic switches (Huberts et al., 2015).

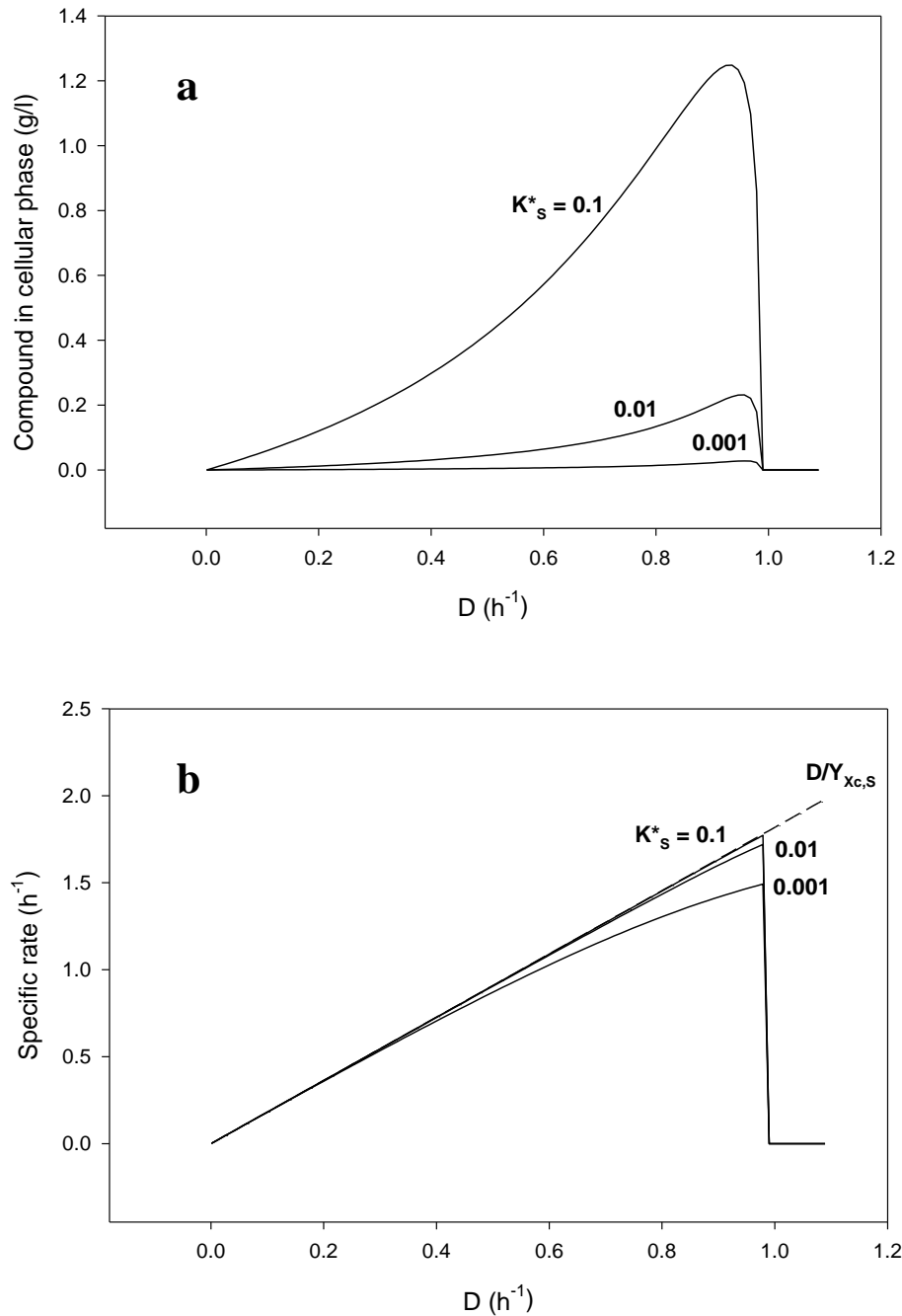


Figure 1. (a) Compound pseudo-homogeneous concentration in cellular phase versus dilution rate. Generator model parameters (Monod): $\mu_{max} = 1$; $K_M = 0.1$; $Y_M = 0.55$; $S^0 = 10$. PDS parameters: $V_S^0 = 2$ (h⁻¹); $K_S^* = 0.1, 0.01, 0.001$ (see curves). (b) Specific transport/metabolization rate versus dilution rate. Generator model parameters (Monod): as in Figure 1a. PDS parameters: as in Figure 1a.

Transition (threshold)

The true discontinuous situation only occurs when affinity is infinite and when the T/M rate is lower than the washout.

For $K_S^* = 0$, the solution (Equation 20) is as follows:

$$\tilde{C}_S^c = \frac{-a_1 + |a_1|}{2a_2} \quad (23)$$

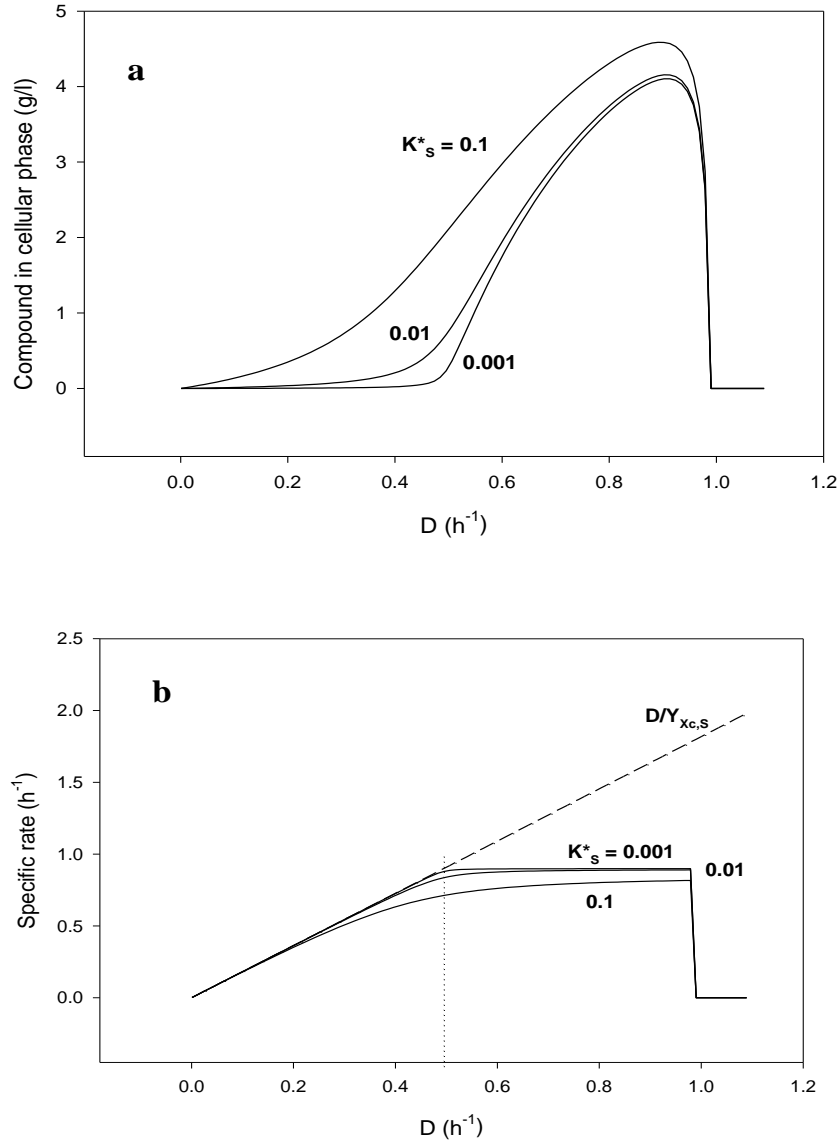


Figure 2. (a) Compound pseudo-homogeneous concentration in cellular phase versus dilution rate. Generator model parameters (Monod): as in Figure 1a. PDS parameters: $V_S^0 = 0.9$ (h^{-1}); $K_S^* = 0.1, 0.01, 0.001$ (see curves). (b) Specific transport/metabolization rate versus dilution rate. Generator model parameters (Monod): as in Figure 1a. PDS parameters: as in Figure 2a.

The concentration in the cellular phase vanishes if $a1 < 0$ and becomes positive if $a1 > 0$:

$$\tilde{C}_S^c = \frac{\Phi_S^0 - V_S^0 X^c}{D}$$

Under these conditions, it is obvious that the threshold value occurs for $a1 = 0$, that is, when

$$\Phi_S^0 = X^c V_S^0 \tag{24}$$

This relation expresses that abrupt transition takes place when the interphasic exchange flux becomes equal to the maximum T/M flux ($X^c V_S^0$). Using Equations 4 and 11, it is easy to calculate D_c from Equation 24 and

$$D_c = V_S^0 Y_{X^c,S} \tag{25}$$

This relation is very important because it shows the relation between the critical dilution rate (threshold) and the global and intrinsic characteristics of the culture,

namely, the total yield coefficient (which is here a constant equal to Y_M) and the maximum T/M rate. The relation (Equation 25) is only exact for $K_S^*=0$ but remains a very suitable approximation for $K_S^*\ll 1$. It is obvious that the threshold phenomena are only observable if the critical dilution rate value is lower than the washout.

In a system such as this, it appears that a compound that can be transported and metabolized in the cellular phase may be maintained with extremely low intracellular concentrations at low dilution rates and may accumulate when the dilution rate reaches a critical value.

The conditions required for the occurrence of such a phenomenon are: (a) that T/M obeys kinetics like Equation 16; (b) that the maximum T/M specific rate is lower than the washout; (c) that the affinity for the compound is sufficiently high.

If the compound is active (at a genetic, enzymatic, or other level), we will be able to take the abrupt physiological changes into account by using the present model.

$n=2$: Two ways model

To shorten the present analysis, a system with two particular pathways will be considered: a low maximum specific rate and high-affinity pathway and a very low-affinity pathway. This situation is very often observed in reality (Walker, 1998; Postma et al., 1989). The case of a pathway with high affinity has been presented in the preceding section and can be represented by:

$$q_S^c(h) = \frac{V_S^0 \tilde{C}_S^c}{K_S^* X^c + \tilde{C}_S^c} ; K_S^* \ll 1 \quad (26)$$

where h indicates the high-affinity kinetics.

The other pathway is expressed in R-concentrations by the general relation (Equation 14):

$$q_S^c(2) = \frac{V_S^0(2) C_S^c}{K_S(2) + C_S^c} \quad (27)$$

A system where affinity is sufficiently low was chosen so that:

$$K_S(2) \gg C_S^c \quad (28)$$

The relation (Equation 27) then look like a kinetics of order 1:

$$q_S^c(2) \approx k_0 C_S^c \quad (29)$$

where $k_0 = V_S^0(2)/K_S(2)$.

Changing from R- to E-concentrations, like before, we obtain the expression of the T/M specific rate for the low-affinity pathway, l :

$$q_S^c(l) = k_0^* \frac{\tilde{C}_S^c}{X^c} \quad (30)$$

where $k_0^* = k_0 \delta_c$.

The total rate is then the sum of two components (Equations 26 and 30):

$$q_S^c = q_S^c(h) + q_S^c(l) = \frac{V_S^0 \tilde{C}_S^c}{K_S^* X^c + \tilde{C}_S^c} + \tilde{C}_S^c k_0^* \quad (31)$$

The mass balance in the steady state is therefore (Equation 2):

$$\Phi_S^0 = \frac{V_S^0 \tilde{C}_S^c}{K_S^* X^c + \tilde{C}_S^c} X^c + \tilde{C}_S^c (k_0^* + D) \quad (32)$$

The second degree with variable coefficients associated polynomial is

$$P^2(\tilde{C}_S^c) = a'_2 (\tilde{C}_S^c)^2 + a'_1 \tilde{C}_S^c + a_0 = 0 \quad (33)$$

with

$$\begin{aligned} a'_2 &= -K_S^* X^c \Phi_S^0 \\ a'_1 &= X^c (V_S^0 + K_S^* (D + k_0^*)) - \Phi_S^0 \\ a'_0 &= D + k_0^* \end{aligned} \quad (34)$$

Equation 33 has the same properties as Equation 18 and only admits one not negative real solution:

$$\tilde{C}_S^c = \frac{-a'_1 + \sqrt{a_1'^2 - 4a'_2 a'_0}}{2a'_2} \quad (35)$$

Figures 3a and b show the most significant differences between the 1 and 2 pathways models.

Concentration in the cellular phase can be decreased while increasing k_0^* . The low-affinity pathway thus makes it possible to control the quantity of product in the cell (Figures 3a and 2a). The total specific T/M rate undergoes no saturation phenomenon anymore. This rate and their two components (low and high) are as shown in Figure 3b. In this example, it clearly appears that for $D < D_c$, the compound concentration in the cellular phase is almost zero. Consequently, the specific T/M rate is also almost zero, as it is a first order kinetic reaction. The

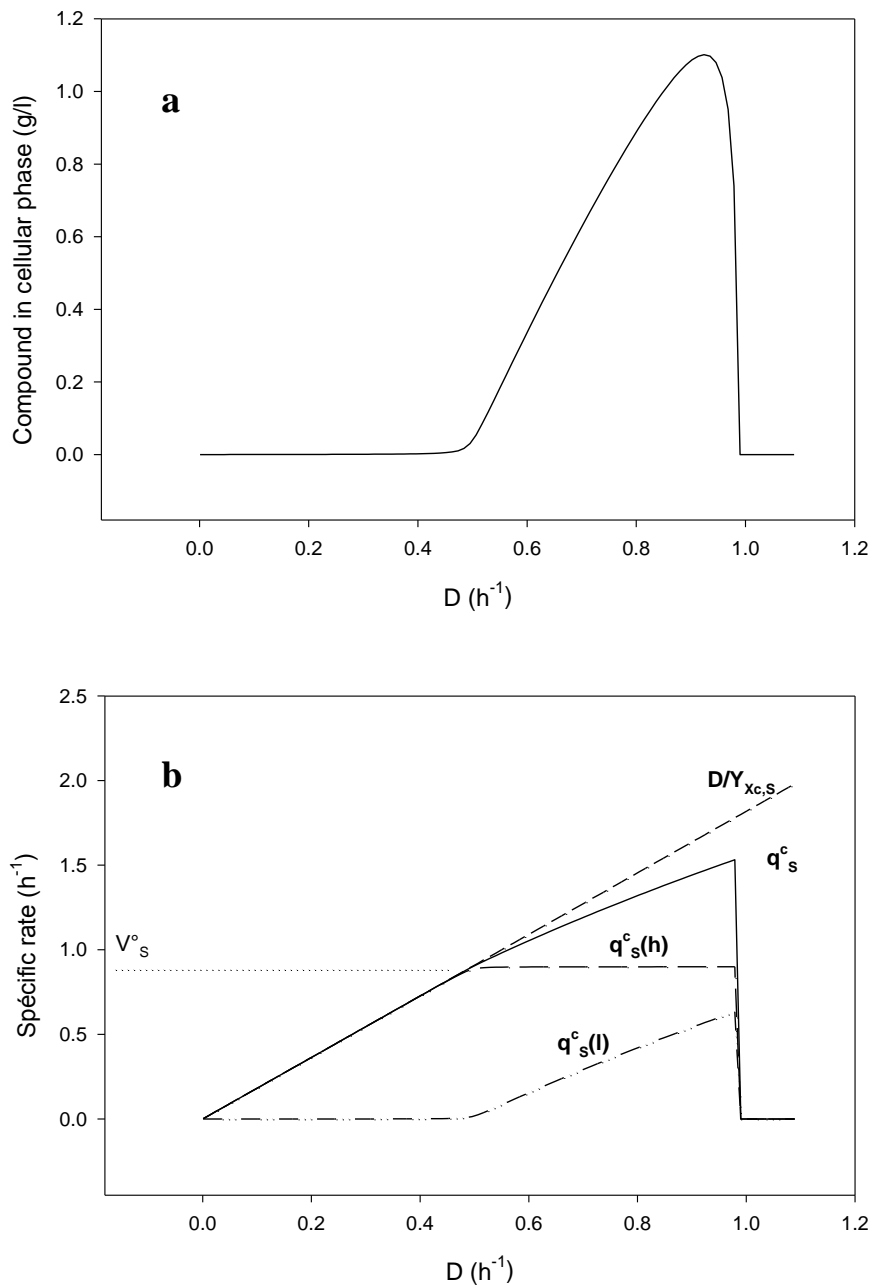


Figure 3. (a) Compound pseudo-homogeneous concentration in cellular phase versus dilution rate. Generator model parameters (Monod): as in Figure 1a. PDS parameters: $V_s^0 = 0.9$ (h^{-1}); $K_S^* = 1.10^{-4}$; $k_0^* = 2.5$ (h^{-1}). (b). Specific transport/metabolization rate versus dilution rate. Generator model parameters (Monod): as in Figure 1a. PDS parameters: as in Figure 3a.

high-affinity pathway, because of its hyperbolic form, can take a significant value, even for low concentrations (as long as the affinity term is of the same order of magnitude as the concentration, which is the case with high affinities).

Beyond D_c , the “high affinity” pathway rate saturates,

like previously, but the “low affinity” pathway takes significant values, linearly depending on D . With parameters used in this example, the total specific rate is close to its maximum for $D < D_c$ and diverges from this value when D increases. Globally, this situation is comparable to the situation represented in Figure 1b, but

the mechanisms concerned are completely different. It should be noted that the one-way model is only a particular case of the two ways model when $k_0^* = 0$. The remark made about the flux-sensing substrate made for the previous case is obviously even more true for the $n = 2$ case.

Transition (threshold)

As described previously, it can be shown that the transition is carried out for $a'_1 = 0$. This relation follows:

$$\Phi_S^0 = X^c (V_S^0 + K_S^* (D + k_0^*)) \quad (36)$$

With high affinities, relation (Equation 36) reduces to

$$\Phi_S^0 \approx X^c (V_S^0 + K_S^* k_0^*) \quad (37)$$

The last term of this relation has a significant value only if k_0^* is very large (approximately the magnitude of the inverse of K_S^*). Under these conditions, Equation 37 infers that the transition occurs when the interphasic exchange flux is equal to the maximum flux of the high-affinity pathway plus a cross term ($X^c K_S^* k_0^*$), thus highlighting an interaction between the two ways. However, this situation is yet to be observed in practical examples, and it is probable that the approximation:

$$\Phi_S^0 \approx X^c V_S^0 \quad (38)$$

is generally sufficient.

Concerning the critical dilution rate, one shows that, with high affinities:

$$D_c = \frac{V_S^0 + K_S^* k_0^*}{1/Y_{X^c,S} - K_S^*} \quad (39)$$

What reduced to:

$$D_c \approx (V_S^0 + K_S^* k_0^*) Y_{X^c,S} \quad (40)$$

corresponding to Equation 37. Again, it is probable that the following approximation will be sufficient in many cases:

$$D_c \approx V_S^0 Y_{X^c,S} \quad (41)$$

an equal value to the one obtained in the one-way model (Equation 25).

This relation may be of great practical importance in terms of modifying the critical value (by acting on mediums, by genetic engineering, etc).

A system of which the total specific T/M rate is made up of two terms (high and low affinities) is able to switch abruptly from a metabolic mode to another when a critical (threshold) dilution rate is reached. In the present case, the "low affinity" pathway is abruptly activated simultaneously, while the "high affinity" pathway takes a constant value ("deactivation"). Beyond the threshold, the compound concentration increases in the cellular phase.

According to the nature of the compound, this effect can involve consequences on other metabolic pathways and act as a "chemical" signal at the cellular level. It is interesting to note that the introduced concept significantly differs from the one considered for the "intercellular communication." For example, Decho (1999) described quorum sensing by circulation of the homoserine lactone effector that penetrates cells via diffusion. The effectors would be inactive until they bind to the receptors, and this event would be triggered beyond a critical threshold concentration in the extracellular medium. In the present approach, an additional condition appears, that is, the physiological state of the cell. The signal would not be solely activated according to the external concentration but would also depend on the metabolization rate of the effector in the cell. In the present case, identical cells with different growth rates would not necessarily give the same response to a common effector, even for identical extracellular concentrations.

Two ways model with a compound release

To address more complex cases, it is necessary to consider a situation in which a part of the compound entered in the cellular phase is released. As such, this situation has only little interest here, but it is a required step for the analysis.

Considering again the mass balance (Equation 32) in its implicit form:

$$\Phi_S^0 - (q_S^c(h) + q_S^c(l)) X^c - D \tilde{C}_S^c = 0 \quad (42)$$

and assuming that part of the intracellular flux of the low-affinity pathway is excreted; let

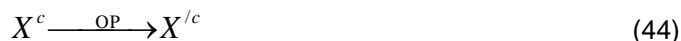
- (1) $\beta q_S^c(l) X^c$ the fraction which remains in the cellular phase and
- (2) $(1 - \beta) q_S^c(l) X^c$ the excreted fraction, be, with necessarily $0 \leq \beta \leq 1$.

With part of the excreted compound, it would be necessary to write the mass balance in the form:

$$\Phi_S^0 - (q_S^c(h) + \beta q_S^c(l)) X^c - D \tilde{C}_S^c = 0 \quad (43)$$

Simulations show that Equation 43 involves a violation of Equation 9 (data not shown) and that the total T/M specific rate exceeds its maximum rate when $D > D_c$. Mass balances (Equations 42 and 43) are however formally correct, but Equation 43 infringes one of the conditions on the maximum specific rate when Monod's generator model is used (Equations 21a and b).

In order to satisfy the two balances simultaneously, we must identify an operator that acts on the biomass to change it:



This operator is easy to find, as the modified biomass must also satisfy the balance (Equation 42). One can therefore easily derive from this relation that:

$$X^{/c} = \frac{\Phi_s^0 - D\tilde{C}_s^c}{q_s^c(h) + q_s^c(l)} \quad (45)$$

By comparing Equation 42 with (modified biomass) and Equation 43, we can show that

$$\frac{X^{/c}}{X^c} = \frac{q_s^c(h) + \beta q_s^c(l)}{q_s^c(h) + q_s^c(l)} \leq 1 \quad (46)$$

and thus, that the adjustment consists in a biomass decrease, compared to the generator model. In concrete terms, the transformation (Equation 44), which consists of modifying the biomass to restore a mass balance disturbed by a compound "release," amounts to partially uncoupling the compound metabolization and the biomass production. This process applies to specific compounds: the substrates. In other words, the relation (Equation 45) allows the amount of biomass produced to be calculated when part of the substrate is diverted from the biosynthesis pathways (anabolism and fueling). Figure 4 shows the result of transformation (Equation 45). It is obvious that the threshold D_c and the washout value are unchanged. The higher the affinity, the steeper the decrease in biomass. Figure 5 shows the specific rates profiles. On this side, the threshold, the total specific rate is unchanged compared to the simple two ways model, as the "low affinity" component is inactive. Beyond the threshold, the total specific rate abruptly increases, since the interphasic flow is unchanged (it does not depend on release) and biomass decreases significantly (due to release). This accounts for the fact that the same substrate flux is "treated" by a smaller amount of biomass and therefore, there is an increase in the specific rate (flux per biomass unit). It is important to note that the simulation that generated the results in Figure 4 does not require any conditional test or optimization condition over the course of the program.

The algorithm is as follows:

Beginning ($D = 0$) calculate the substrate S via a generator model or use a fitting of the experimental data

-calculate: $X^c = Y_M(S^0 - S)$

-obtain \tilde{C}_s^c via (Equation 32)

-calculate $q_s^c(\tilde{C}_s^c, \dots)$ via (Equation 31)

-calculate $X^{/c}$ via (Equation 35)

-increment D and return at the first step

End ($D = D_w$)

The yield coefficient used in the algorithm is that of the generator model that allows evaluating X^c . Notably, the true yield coefficient is not a constant on the whole interval of D ; it is calculated by using the usual relation (Equation 4) with the $X^{/c}$ value.

For the determination of D_c , the relevant value of the yield coefficient is that obtained for $D < D_c$ in the absence of a maintenance term $Y_{X^c, S} = Y_{X^{/c}, S} = Y_M$.

Metabolites excretion

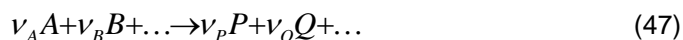
In the preceding section, we considered a release of the substrate from the cellular phase.

Although this phenomenon can be envisaged (Thierie, 2000), the substrate is not generally excreted in its unaffected form. In particular, in fermentation phenomena, part of the substrate, diverted from biosynthesis and fueling flux, is transformed by oxidoreductive reactions and is excreted in another form. It is this type of phenomenon that we would like to consider here. Before addressing subject, it is advisable to introduce some general concepts.

General

In the PDS approach, all flux and concentrations are expressed in term of mass. Relations mainly between mass and molar formalism were introduced here.

For any general chemical reaction like



there are two basic relations (for sake of simplicity, we will use the subscript alone in place of the compound symbol: $i=P_i$):

$$\sum_i v_i M M_i = 0 \quad (48)$$

that expresses the molecular mass balance, with $M M_z$ the Z compound molar mass and v_z his stoichiometric coefficient (negative definite on the left and positive on the right).

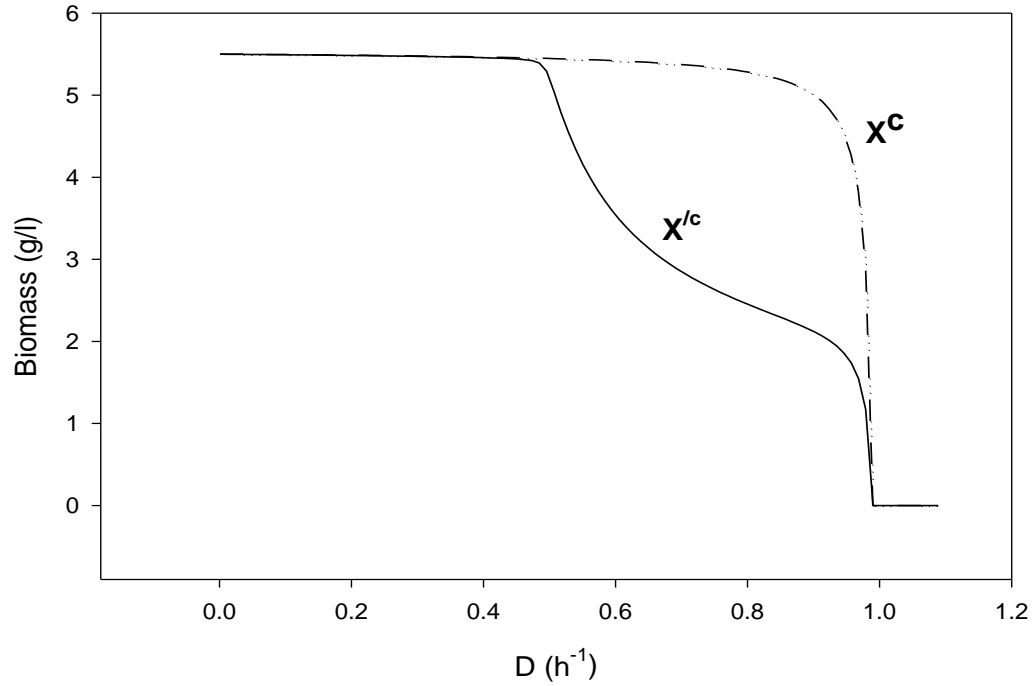


Figure 4. Biomass versus dilution rate. Transformation (15) generates an abrupt biomass decrease in the steady state for $D > D_c$ (full line). The generator model biomass exhibits its usual (Monod's) profile (dashed line). The two critical values D_c and D_W are preserved. Generator model parameters (Monod): as in Figure 1a. PDS parameters: $v_s^0 = 0.9 \text{ (h}^{-1}\text{)}$; $K_s^* = 1.10^{-4}$; $k_0^* = 2.5 \text{ (h}^{-1}\text{)}$; $\beta = 0.2$.

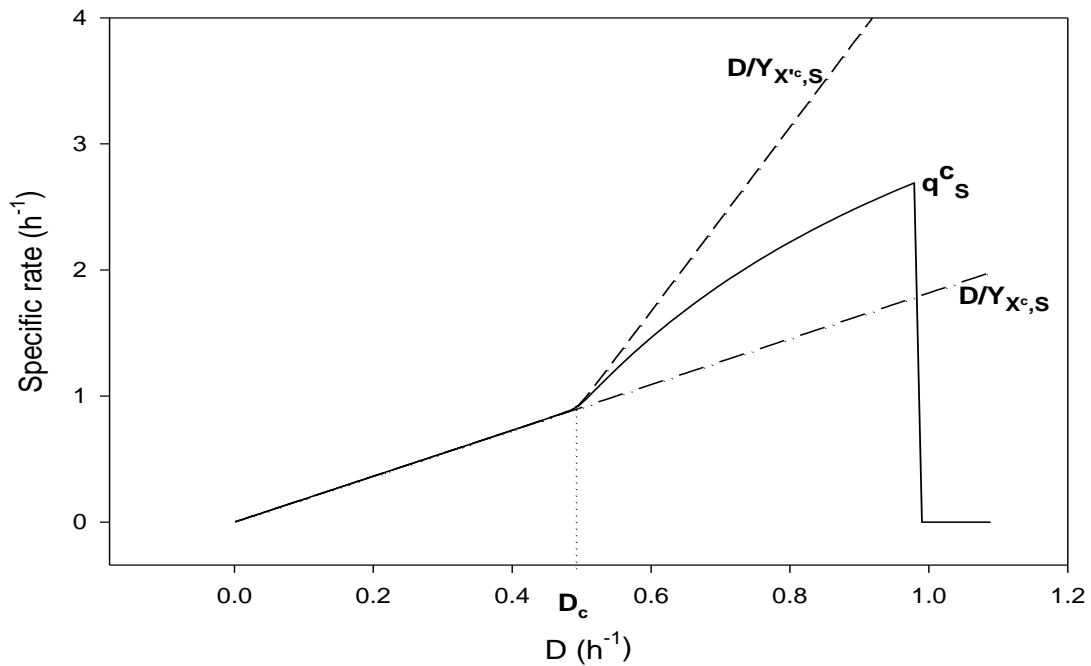


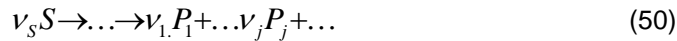
Figure 5. Specific transport/metabolization rate versus dilution rate. Global specific rate, as well as its maximal values before and after the transition, are represented. For $D > D_c$, the specific rate is significantly higher than its maximal value before the transition. Biomass adjustment (45) leads to a sudden increase of the total specific rate maximal value. Generator model parameters (Monod): as in Figure 1a. PDS parameters: as in Figure 4.

In addition, for each couple of compounds:

$$\frac{n_i}{n_j} = \left| \frac{v_i}{v_j} \right| \quad (49)$$

where n_z is the number of moles of compound Z (the molar ratio being always positive, it is necessary to use the absolute values of the stoichiometric coefficients). This relation expresses that the ratio of the numbers of moles is equal to the ratio of the stoichiometric coefficients.

Now let us consider a particular case from Equation 47.



This equation only represents the initial reagent (S) and all the products (P_j), independent of the intermediate compounds and the path followed to obtain the final compounds. Equation 48 can be put in the form:

$$-v_S MM_S = \sum_j v_j MM_j \quad (j \neq S) \quad (51)$$

Dividing by MM_S , it follows:

$$1 = - \sum_j \frac{v_j MM_j}{v_S MM_S} \quad (j \neq S) \quad (52)$$

Let us define the positive value:

$$\rho_{j,S} = \left| \frac{v_j MM_j}{v_S MM_S} \right| \quad (53)$$

Here are the following properties:

$$\sum_j \rho_{j,S} = 1 \quad (54)$$

$$\rho_{j,S} = \frac{1}{\rho_{S,j}} \quad (55)$$

Using relation between mole and mass:

$$n_k = \frac{M_k}{MM_k} \quad (56)$$

where M_k is the mass of the compound K ; in relation (Equation 49), we report that for each product:

$$\frac{M_i}{M_S} = \left| \frac{v_i MM_i}{v_S MM_S} \right| \quad (57)$$

Comparing with Equation 53,

$$\rho_{i,S} = \frac{M_i}{M_S} \quad (58)$$

will be referred to as the mass coefficient ratio (MCR).

Application to concentrations

Putting Equation 58 in the form

$$M_i = \rho_{i,S} M_S \quad (59)$$

with constant volume

$$\tilde{C}_i^x = \rho_{i,S} \tilde{C}_S^x ; \quad x=c,m,\dots \quad (60)$$

This relation obviously extends to other types of concentrations, R-concentrations, etc.

Application to specific rates

The relation (Equation 58) can be transformed into the following identity:

$$\frac{\Delta M_i}{\Delta t X^{1/c}} \frac{\Delta t X^{1/c}}{\Delta M_S} = \rho_{i,S} \quad (61)$$

In the balances, the specific rates are positive definite (with appropriate sign). One can thus assume that, for a single cellular scheme like (Equation 50):

$$\lim_{\Delta t \rightarrow 0} \frac{\Delta M_k}{\Delta t X^{1/c}} \equiv q_k^x ; \quad x=m,c,\dots \quad (62)$$

and Equation 61 becomes

$$\frac{q_i^x}{q_S^x} = \rho_{i,S} \quad (63)$$

A particular form of Equation 63 is as follows:

$$q_i^c = \rho_{i,S} q_S^c \quad (64)$$

the equivalent form of it, in our usual formalism, is

$$q_{P_i}^c = \rho_{i,S} q_S^c \quad (65)$$

Mass balances

In the cellular phase, each product (or metabolite)

excreted is characterized by the balance:

$$\frac{d\tilde{C}_{P_i}^c}{dt} = \Pi_{P_i}^c - \Phi_{P_{i,c}}^0(m) - D\tilde{C}_{P_i}^c + \tilde{C}_{P_i}^c \frac{d \ln N_T^c}{dt} \quad (66)$$

where

$\Pi_{P_i}^c$ is a production flux (for example, directly from the substrate, as in the scheme (Equation 50)). $\Phi_{P_{i,c}}^0(m)$ is the net (input/output balance) excreted product flux from the cellular phase towards the matric phase.

The other terms keep their former meaning. In the matric phase, if P_i does not undergo any transformation ($R_{P_i}^m = 0$), the mass balance is:

$$\frac{d\tilde{C}_{P_i}^m}{dt} = \Phi_{P_{i,c}}^0(m) - D\tilde{C}_{P_i}^m \quad (67)$$

The steady state corresponding to Equation 66 implies that

$$\Phi_{P_{i,c}}^m(m) = \Pi_{P_i}^m - D\tilde{C}_{P_i}^c \quad (68)$$

that expresses the excreted flux is equal to the production flux minus the hydraulic output term of the product associated with the cellular phase. In the same way, Equation 67 gives

$$\Phi_{P_{i,c}}^0(m) = D\tilde{C}_{P_i}^m \quad (69)$$

expressing that the excretion flux is balanced by the hydraulic output in the matric phase.

Combining Equation 68 and 69 lead to

$$\Pi_{P_i}^c - D(\tilde{C}_{P_{i,c}}^c + \tilde{C}_{P_{i,c}}^m) = 0 \quad (70)$$

For systems where biomass is not too high and where product accumulation in the cellular phase is low, it is reasonable to assume that

$$\tilde{C}_{P_i}^c \ll \tilde{C}_{P_i}^m \quad (71)$$

This assumption does not imply that the actual intracellular concentration is negligible, but rather it implies that the pseudo-homogeneous concentration in the cellular phase is negligible in relation to the concentration in the medium.

When Equation 71 is applied, the relation (Equation 70) admits the approximate form:

$$\Pi_{P_i}^c \approx D\tilde{C}_{P_i}^m \quad (72)$$

This relation establishes the link between the production flux in the cellular phase and the metabolite concentration excreted in the matric phase. From this, it may be deduced that

$$\tilde{C}_{P_i}^m = \frac{\Pi_{P_i}^c}{D} \quad (73)$$

Relationship to kinetics expressed in term of substrate

To evaluate the metabolite production based on kinetics expressed in terms of the substrate, it is necessary to establish the link between "substrate-equivalent" and product.

A flux can generally be represented by the product of a specific rate and the biomass:

$$\Pi_{P_i}^c = q_{P_i}^c X^{1/c} \quad (74)$$

The link between the specific excreted metabolite production rate and the corresponding substrate disappearance rate is then given by Equation 65. Using this relation and combining Equations 73 and 74, one obtains (for a scheme like (Equation 50)).

$$\tilde{C}_{P_i}^m = \rho_{P_{i,S}} q_S^c(*) X^{1/c} / D \quad (75)$$

It is obvious that all the substrate "treated" in the cellular phase will not be excreted as metabolites. $q_S^c(*)$ represents thus the specific rate fraction devoted to the production of metabolites P_i . Relation (Equation 75) is general in the sense that it does not depend on a precise model (it is an implicit form). The explicit form of Equation 75 can be obtained by using the excreted fraction as defined earlier. This can be expressed as follows:

$$\tilde{C}_{P_i}^m = \rho_{P_{i,S}} (1 - \beta) q_S^c(l) X^{1/c} / D \quad (76)$$

This relation gives the possibility to calculate the metabolite concentration excreted in the matric phase on a T/M substrate kinetics basis. It is obviously a fundamental result for the evaluation of the model validity when applied to a process involved in growth and substrate utilization decoupling. Fermentation processes are good examples of applications. As an illustration, the Figure 6 shows the profile of the concentrations of the excreted products. Curve (1) shows the excretion in substrate-equivalent ($\rho_{P,S} = 1$) and curves (2) and (3), respectively show those of hypothetical products accounting for 3/4 and 1/4 of the substrate mass ($\rho_{P_{1,S}} = 0.75$ and $\rho_{P_{2,S}} = 0.25$). The curves are qualitatively in agreement with the profiles typically

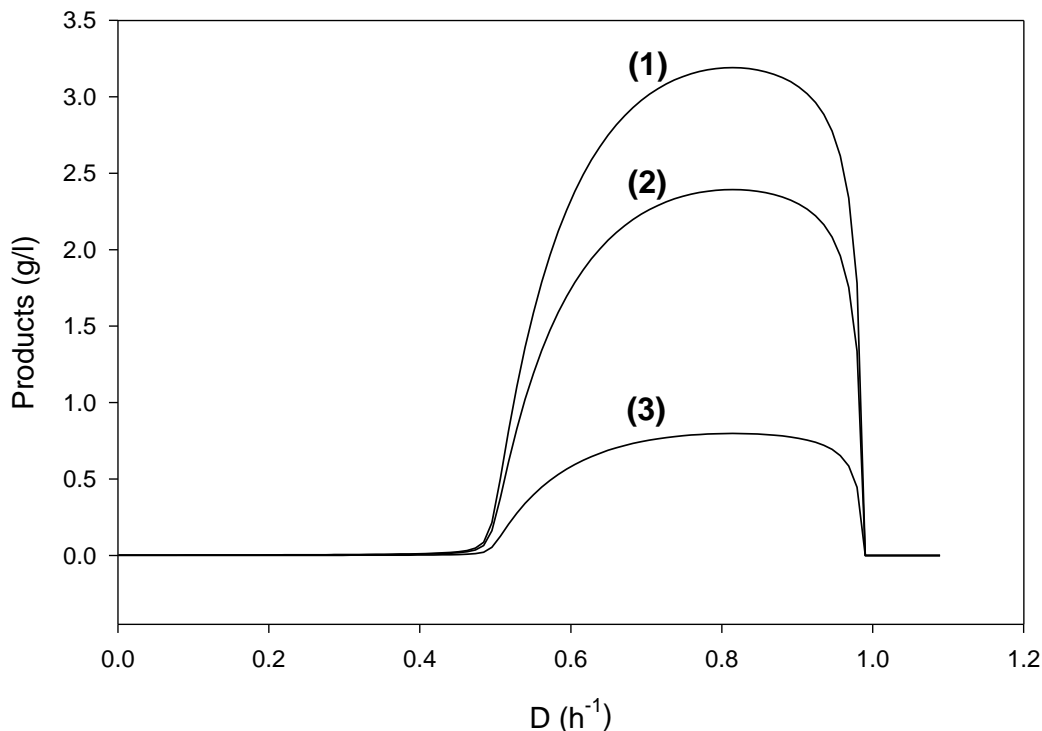


Figure 6. Excreted products concentration in matric phase versus dilution rate. Curve (1) shows the “substrate-equivalent” concentration ($\rho_{P,S}=1$). Curves (2) and (3) correspond to scheme $S \rightarrow P_1 + P_2$ with $\rho_{P_1,S}=0.75$ and $\rho_{P_2,S}=0.25$. The substrate is decomposed into two products, P_1 and P_2 , with hypothetical mass ratio coefficients equal to $\frac{3}{4}$ and $\frac{1}{4}$, respectively. Generator model parameters (Monod): as in Figure 1a. PDS parameters: as in Figure 4.

observed in a chemostat. Corresponding specific rate (not represented) vary in an increasing monotonous way with D beyond the critical value and vanish in on this side. They tend to adopt a straight line when k_0^* is large enough.

In all cases exhibiting a threshold phenomenon presented here, it is always possible to calculate a “substrate threshold value.” It is the value for which $D=D_c$ in (21a). This latter relation is continuous for dilution rates lower than washout. Therefore, expressing the threshold in term of the substrate has no real significance, according to from our point of view. Moreover, Equation 21a is not ideal for fitting experimental data. Besides, inaccuracy of residual substrate measurements in this range of D would prevent this measurement from being operational.

DISCUSSION

From a conceptual point of view, the statement that merits increased recognition is the expression of the transport/metabolization kinetics (T/M) using pseudo-

homogeneous concentrations (E-concentrations) initially obtained in terms of local concentrations (R-concentrations) (Thierie, 1997).

In a polyphasic representation, the kinetics of T/M describes an interfacial process and is therefore heterogeneous. This situation already poses the problem of defining “efficient” concentrations (Villermaux, 1982; Roels, 1983). Coulson and Richardson (1987) discussed the local form (Equation 14) for $n=1$. They concluded that this relation appropriately expresses both substrate transport, as well as substrate metabolization, if the maximum metabolization rate is higher than the transport rate. However, this condition is too restrictive, as it excludes the possibility of “free substrate” accumulation in the cell. Moreover, the hyperbolic form of Equation 14 reflects the phenomenon of transport by diffusion (facilitated or not) well (Walker, 1998; Schechter, 1997) and is regularly used to model other mechanisms of transport. The local form of the phenomenon of T/M, expressed in term of R-concentration, can thus be considered as adequate. On the other hand, the total global forms reveal dependence between local kinetics and biomass. The similarity between the concepts suggested by Abbott and Nelsestuen (1988) and the

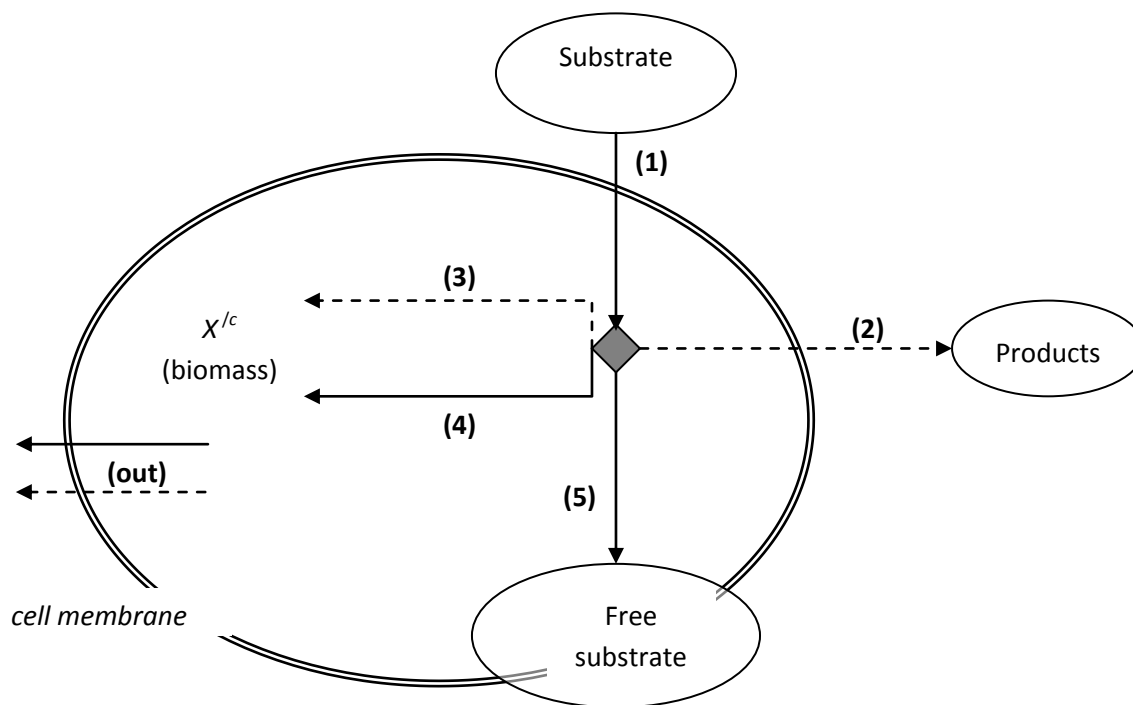


Figure 7. Main specific rates distribution in cellular phase (presented here as an “isolated cell”). (1) Total T/M specific rate: $q_s^c = q_s^c(h) + q_s^c(l)$; (2) excretion $(1-\beta)q_s^c(l)$; anabolism/fueling: (3) $\beta q_s^c(l)$ and (4) $q_s^c(h)$; (5) Free substrate: $D\tilde{C}_s^c/X^{/c}$; (out) output term taking the yield coefficient (not quantified) into account. Dashed lines show metabolic pathways only activated for $D > D_c$.

results obtained in this study using a different approach are briefly outlined here. The authors showed that if the number of cellular receptors is high (about 10% of membrane surface), the rate of formation of the receptor-ligand complex no longer depends on receptors concentration, but on the cellular concentration. The authors refer to this situation as “the collisional limit.” Moreover, the authors showed that, for hyperbolic kinetics, the collisional limit involved a variation of affinity based on the number of cells.

In our model, the resultant affinity ($K_s^* X^{/c}$) is a decreasing function of the biomass, if K_s^* is a true constant and if δ_c only varies slightly with the culture conditions, which can be regarded as reasonable (Kubitschek et al., 1983; Kubitschek et al., 1984; Baldwin and Kubitschek, 1984). In addition, other studies in several experimental situations supported the influence of biomass on substrate affinity (Contois, 1959; Roques, 1982). It is possible that these problems are complicated and have not been resolved as of yet. While waiting for a unified interpretation, we can consider the kinetics used here as a useful phenomenological representation of the T/M kinetics, as it has been tested successfully on various cases (unpublished results). Finally, it is reasonable to conclude that the division of a substrate

among a large number of cells requires a representation that considers the interaction between the cells. The independence of cells growing on a common substrate is intuitive only for very low cellular concentration systems where cells can be regarded as isolated from one another.

Taken as a whole, the one or two pathways models make it possible to give an account of “signaling” phenomena appearing at a critical dilution rate once a transported and partially metabolized compound has entered the cell. The abrupt increase in an intracellular effector concentration is likely to trigger activation at the enzymatic, as well as genetic levels. The present algorithm accounts for such a situation and does not require any *ad hoc* preconditions or preliminary constraints. When metabolite excretion is considered, our approach enables a model of the decoupling between substrate consumption devoted to growth and the fraction used for other factors such as excretion of fermentation products. This last approach is particularly fruitful, as it leads to the possibility of visualizing the distribution of the principal specific rates (or principal flux) of the substrate metabolism. Figure 7 shows a way of representing this distribution in the cellular phase (showed as a simple cell).

The arrow (1) indicates the total substrate T/M flux (two pathways model). The high-affinity pathway (4) is

permanent and feeds anabolism and fueling pathways (with an output way (**out**) for water, CO₂, etc. not quantified here). The arrows (2) and (3) represent the low-affinity pathway, which is only triggered beyond the critical point (an exit point (out) is also associated with this mechanism). The arrow (5) represents the free substrate, adsorbed on the membrane and/or present in the cell. In this representation, there is "a nodal point" which represents the connection of the principal pathways of anabolism/fueling, excretion, and free substrate. The dashed lines indicate the pathways which are activated for $D > D_c$. The way (5) may also decrease below the critical point or become negligible on the whole dilution rates interval depending on the value of k_0^* . Overall, for $D < D_c$, only the ways (1) and (4) are active, as all the substrate is used for biosynthesis and fueling reactions. For $D > D_c$, the pathway (4) saturates and reaches its maximum value. Pathways (2), (3), and (5) are activated. Biosynthesis is then ensured via pathways (3) and (4). Pathway (2) is used for substrate transformation and formation of products excreted in the matric phase.

The nodal point of Figure 7 appears to be the "logical" metabolomic location of what is referred to as the overflow (Vazquez, 2018) location. While our model does not explicitly define the overflow mechanism, it does not exclude this denomination. On the other hand, it is more likely to be related to the concept of "valve" actuated by the incoming substrate flux (Huberts et al., 2015) in the respirofermentative transition (Alves-Araújo et al., 2007).

The scheme in Figure 7 was used to describe the Crabtree effect in *Saccharomyces cerevisiae*. In one study case, the specific rates analysis was closer to being complete and was shown to be very effective (unpublished results). The similarity to the Warburg effect (de Alteiisa et al., 2018) paves the way for future applications, particularly in the field of health and cancer.

To conclude, we believe that the model presented here, although able to deal with rather complex phenomena, may have a practical utility for design and optimization of biotechnological and economic problems (such as optimization of fermentation processes) and health problems (for example, links to cancer and Warburg and Crabtree effects). From a more fundamental point of view, the PDS representation has already shown its utility (Thierie, 1997, 2000). The prospects linked to the use of explicit forms of the specific rates are numerous and have already shown great potential in optimization of various processes in the field of biotechnology.

CONFLICT OF INTERESTS

There is no conflict over this article.

REFERENCES

Abbott AJ, Nelsestuen GL (1988). The collisional limit: an important

- consideration for membrane-associated enzymes and receptors. *FASEB Journal* 2(13):2858-2866.
- Afroz T, Biliouris K, Kaznessis Y, Beisel CL (2014). Bacterial sugar utilization gives rise to distinct single-cell behaviors. *Molecular Microbiology* 93(6):1093-1103.
- Alves-Araújo C, Pacheco A, Almeida MJ, Spencer-Martins I, Leão C, Sousa MJ (2007). Sugar utilization patterns and respiro-fermentative metabolism in the baker's yeast *Torulaspora delbrueckii*. *Microbiology* 153:898-904
- Baldwin WW, Kubitschek, HE (1984). Buoyant density variation during the cell cycle of *Saccharomyces cerevisiae*. *Journal of Bacteriology* 158:701-704.
- Bellgardt KH (1991). Cells Model. In: *Biotechnology* (Rehm, H.J. & Reed, G. with Pühler, A & Stadler, eds) (K. Schügerl, ed) Weinheim: VCH. 4:267-298.
- Contois DE (1959). Kinetics of bacterial growth: relationship between population density and specific growth rate of continuous cultures. *Journal of General Microbiology* 21:40-50.
- Coulson JM, Richardson JF (1987). *Chemical engineering* (Second edition.) UK: Pergamon Press.
- de Alteiisa E, Carten F, Parascandolac P, Serpad J, Mazzolenib S (2018). Revisiting the Crabtree/Warburg effect in a dynamic perspective: a fitness advantage against sugar-induced cell death. *Cell Cycle* 17(6):688-701.
- Decho AW (1999). Chemical communication within microbial biofilms: chemotaxis and quorum sensing in bacterial cells. In: *Microbial extracellular polymeric substances* (Wingender J, Neu TR, Flemming H-C eds.) Berlin: Springer-Verlag. pp. 155-165.
- Degnan PH, Barry NA, Mok KC, Taga ME, Goodman AL (2014). Human gut microbes use multiple transporters to distinguish vitamin B₁₂ analogs and compete in the gut. *Cell Host Microbe* 15(15):47-57.
- Doran PM (1995). *Bioprocess engineering principles*. London: Academic Press.
- Dzialo MC, Park R, Steensels J, Lievens B, Verstrepen KJ (2017). Physiology, ecology and industrial applications of aroma formation in yeast. *FEMS Microbiology Reviews* 41:95-128.
- Foundations of Computer Aided Process Design (FOCAPD) (2004). (Sixth International Conference on Foundations of Computer-Aided Process Design Discovery through Product and Process Design July 11-16, 2004, Princeton, New Jersey.
- Giuseppin MLF, van Riel NAW (2000). Metabolic modeling of *Saccharomyces cerevisiae* using the optimal control of homeostasis: a cybernetic model definition. *Metabolic Engineering* 2:14-33.
- Green ER, Meccas J (2016). Bacterial secretion systems – an overview. *Microbiol Spectrum* 4(1):10.1128/microbiolspec.VMBF-0012-2015
- Gresham D, Hong J (2015). The functional basis of adaptive evolution in chemostats. *FEMS Microbiology Reviews* 39:2-16.
- Huberts DHE, Niebel B, Heinemann M (2015). A flux-sensing mechanism could regulate the switch between respiration and fermentation. *FEMS Yeast Research* 12(2):118-128.
- Kempes CP, van Bodegom PM, Wolpert D, Libby E, Amend J, Hoehler T (2017). Drivers of bacterial maintenance and minimal energy requirements. *Frontiers in Microbiology* 8(31):1-10.
- Koch AL (1997). Microbial physiology and ecology of slow growth. *Microbiology and Molecular Biology Reviews* 61(3):305-318.
- Kubitschek HE, Baldwin WW, Graetzer R (1983). Buoyant density constancy during the cell cycle of *Escherichia coli*. *Journal of Bacteriology* 155:1027-1032.
- Kubitschek HE, Baldwin WW, Schroeter SJ, Graetzer R (1984). Independence of buoyant density and growth rate in *Escherichia coli*. *Journal of Bacteriology* 158:296-299.
- Matteau D, Baby V, Pelletier S, Rodrigue S (2015). A Small-Volume, Low-Cost, and Versatile Continuous Culture Device. *PLoS One* 10(7):e0133384.
- McCoy JG, Elena JL, Zhou M (2015). Structural insight into the PTS sugar transporter EIIC. *Biochimica et Biophysica Acta* 1850(3):577-585.
- Payen C, Dunham MJ (2017). Chemostat culture for yeast experimental evolution. *Cold Spring Harbour Protocols* 7:514-517.
- Pirt SJ (1965). The maintenance energy of bacteria in growing cultures. *Proceedings of the Royal Society B Biological Sciences* 163:224-231.
- Pirt SJ (1982). Maintenance energy: a general model for energy-limited

- and energy-sufficient growth. *Archives of Microbiology* 133:300-302.
- Postma E, Scheffers WA, van Dijken JP (1989). Kinetics of growth and sugar transport in glucose-limited chemostat cultures of *Saccharomyces cerevisiae* CBS 8066. *Yeast* 5:159-165.
- Rapaport A, Tani FZ, Bayen T (2018). Optimal periodic control of the chemostat with Contois growth function. IFAC International Conference on Mathematical Modelling - MATHMOD Vienna, Austria. Elsevier 51(2):730-734.
- Roels JA (1983). Energetics and kinetics in biotechnology. Elsevier Biomedical Press B.V., Amsterdam, New York, Oxford.
- Roques H, Yue S, Saipanich S, Capdeville B (1982). Faut-il abandonner le modèle de Monod pour la modélisation des processus de dépollution biologique ? *Water Research* 16:839-847.
- Schechter E (1997). Biochimie et biophysique des membranes – Aspects structuraux et fonctionnels. Paris: Masson.
- Schügerl K, Bellgardt KH (2000). Bioreaction engineering. Berlin: Springer-Verlag.
- Tempest DW, Neijssel OM (1984). The status of Y_{ATP} and maintenance energy as biologically interpretable phenomena. *Annual Review of Microbiology* 38:459-486.
- Thierie J (1997). Why does bacterial composition change with the chemostat dilution rate?. *Biotechnology Techniques* 11:625-629.
- Thierie J (2000). Cellular cycling of substrate as a possible cryptic way for energy spilling in suspended cellular continuous cultures. *Biotechnology Letters* 22:1143-1149.
- Thierie J (2016). Introduction to Polyphasic Dispersed Systems. Application to Open Systems of Microorganisms' Culture. (Monograph) Springer.
- Varma A, Palsson BO (1993a). Stoichiometric interpretation of *Escherichia coli* glucose catabolism under various oxygenation rates. *Applied and Environmental Microbiology* 59:2465-2473.
- Varma A, Palsson BO (1993b). Metabolic capabilities of *Escherichia coli*: II. Optimal growth patterns. *Journal of Theoretical Biology* 165:503-522.
- Vazquez A (2018). A Historical View of Overflow Metabolism in Overflow Metabolism Elsevier.
- Villermaux J (1982). *Génie de la réaction chimique : conception et fonctionnement des réacteurs*. Technique et Documentation (Lavoisier), Paris.
- Vos T, Hakkaart XDV, Erik AF, de Hulster AJA, van Maris JTP, Daran-Lapujade P (2016). Maintenance-energy requirements and robustness of *Saccharomyces cerevisiae* at aerobic near-zero specific growth rates. *Microbial Cell Factories* 15:111.
- Walker GW (1998). *Yeast – Physiology and biotechnology*. England: John Wiley and Sons.
- Weusthuis RA, Pronk JT, van den Broek PJA, van Dijken JP (1994). Chemostat cultivation as a tool for studies on sugar transport in yeasts. *Microbial Reviews* 58:616-630.
- Zhang J, Miao A, Zhang T (2017). Threshold dynamics of a stochastic chemostat model with two nutrients and one microorganism. *Mathematical Problems in Engineering* Article ID 5217027, 11 p.
- Ziv N, Brandt NJ, Gresham D (2013). The use of chemostats in microbial systems biology. *Journal of Visual Experiments* 80:e50168.